

Anode-Free Sodium Metal Batteries Based on Nanohybrid Core–Shell Templates

Min Eui Lee, Seunggon Lee, Jaewon Choi, Hyoung-Joon Jin, Seungyong Han,*
and Young Soo Yun*

Anode-free sodium metal batteries (AF-SMBs) can deliver high energy and enormous power, but their cycle lives are still insufficient for them to be practical as a power source in modern electronic devices and/or grid systems. In this study, a nanohybrid template based on high aspect-ratio silver nanofibers and nitrogen-rich carbon thin layers as a core–shell structure is designed to improve the Coulombic efficiency (CE) and cycling performance of AF-SMBs. The catalytic nanohybrid templates dramatically reduce the voltage overshooting caused by metal nucleation to one-fifth that of a bare Al foil electrode (≈ 6 mV vs ≈ 30 mV), and high average CE values of $>99\%$ are achieved over a wide range of current rates from 0.2 to 8 mA cm⁻². Moreover, exceptionally long cycle lives for more than 1600 cycles and an additional 1500 cycles are achieved with a highly stable CE of $>99.9\%$. These results show that AF-SMBs are feasible with the nanohybrid electrode system.

Renewable energy systems should contain large-scale energy storage devices (ESDs) to achieve a settled and on-demand energy supply.^[5] In addition, electric vehicles and drones, which are advancing rapidly, call for advanced energy storage devices with higher energy/power densities.^[6,7] The various needs from a compact mobile device to a grid system have accelerated the development of a new type of ESD with high electrochemical performance, such as lithium metal batteries (LMBs),^[8–11] sodium ion/metal batteries,^[12–20] multivalent metal ion batteries,^[21–23] metal–air/sulfur batteries,^[24–28] and organic redox flow batteries.^[29] Among them, LMBs are one of the most promising candidates owing to their high working voltage and

1. Introduction

The change in industrial paradigm caused by the quantum leap in scientific technology requires massive energy consumption, whereas global ecopolicies for environmental issues have strictly limited the use of environmentally hostile technologies.^[1–3] Accordingly, sustainable energy generation technologies based on green energy resources, such as solar, geothermal, wind, and tidal power, are key technologies worldwide.^[1–5]


large theoretical capacities. On the other hand, the poor Coulombic efficiency (CE) and safety issues originating from dendritic metal growth have restricted their application.^[8–11] In addition, the lithium price has risen sharply in recent years because of the insufficient lithium reserves, of which 60% is located in a specific area.^[30] Considering the price issue, sodium metal batteries (SMBs) based on abundant and ubiquitous sodium resources appear to be more suitable. Despite the apparent suitability, SMBs suffer from technological barriers similar to LMBs, which are induced by dendritic metal growth and mossy metal deposits.^[16–20] Therefore, several studies have been conducted to find a means to control undesirable metal growth.^[8–11,16–20] Cui et al. reported dendrite-free metal deposition/stripping cycling with $\approx 99\%$ CE over 150 cycles through the introduction of a carbonaceous interfacial layer.^[8] This allows a uniform lithium ion flux, leading to columnar metal deposition in the space between the carbon-based layer and substrate.^[8] This concept was expanded further by forming an organic or inorganic layer on the lithium metal surface.^[9–11] The coating layer can serve as both a catalyst for metal nucleation and an effective protection barrier against Li metal corrosion, resulting in significantly improved CE and stable cycling.^[9–11] In addition, it was confirmed that an ether-based electrolyte system and/or additives can induce dendrite-free cycling.^[31,32] Under an ether-based electrolyte, the lithiophilic/sodiophilic sites of carbon-based catalytic material (CCM) guide homogeneous metal nucleation, resulting in improved cycling performance.^[19,20,33,34] More functionalized CCMs, including a large number of catalytic sites, exhibited more efficient metal deposition/stripping behaviors, leading to feasible electrochemical

Dr. M. E. Lee, Prof. H.-J. Jin
Department of Polymer Science and Engineering
Inha University
Incheon 402-751, South Korea

S. Lee, Prof. S. Han
Multiscale Bioinspired Technology Lab
Department of Mechanical Engineering
Ajou University
Suwon 16499, South Korea
E-mail: sy84han@ajou.ac.kr

Dr. J. Choi
Institute of Advanced Composite Materials
Korea Institute of Science and Technology (KIST)
92 Chudong-ro, Bongdong-eup, Wanju-gun, Jeonbuk 55324, South Korea

Prof. Y. S. Yun
Department of Chemical Engineering
Kangwon National University
Samcheok 245-711, South Korea
E-mail: ysyun@kangwon.ac.kr

 The ORCID identification number(s) for the author(s) of this article can be found under <https://doi.org/10.1002/sml.201901274>.

DOI: 10.1002/sml.201901274

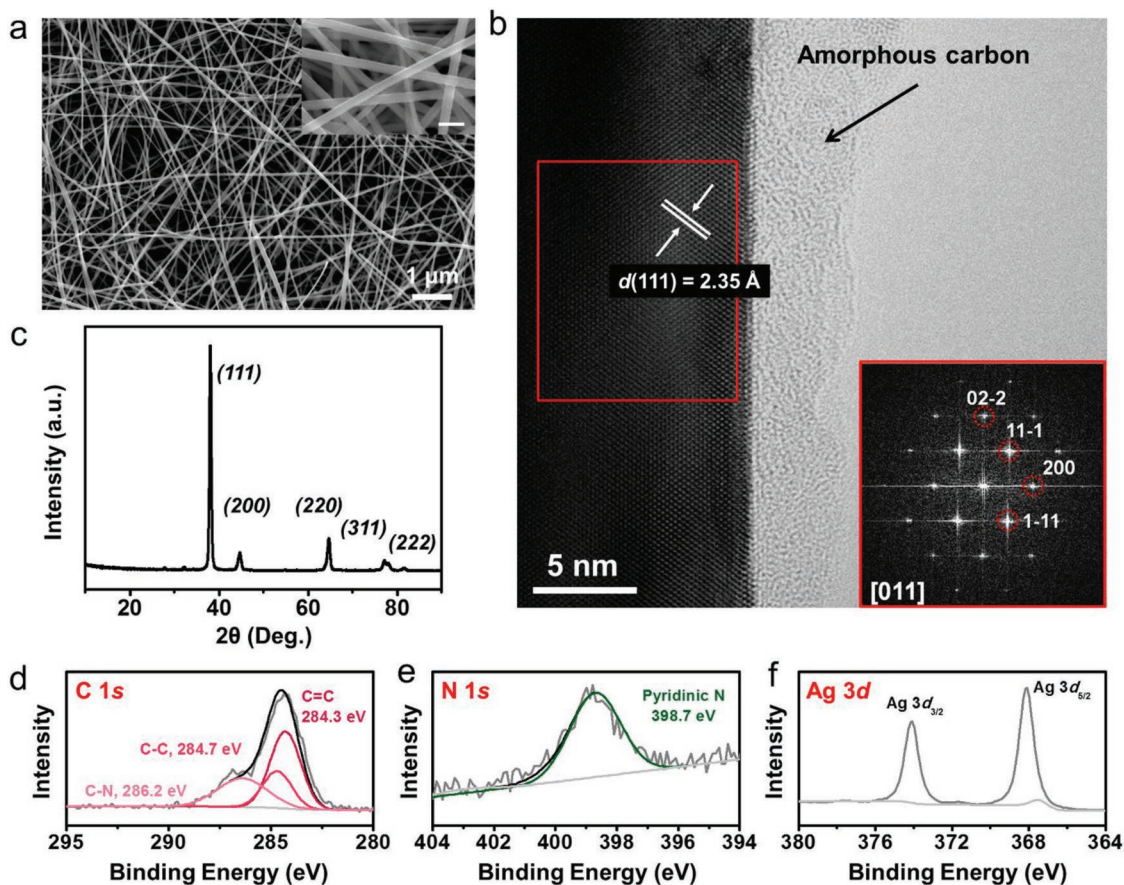


Figure 1. Materials properties of MP-NWBs composed of SNF@NCLs. a) FE-SEM image and inset showing a high resolution FE-SEM image (scale bar: 200 nm), b) FE-TEM image and inset showing a selected area diffraction pattern, c) XRD pattern and XPS, d) C 1s, e) N 1s, and f) Ag 3d spectra.

performance corresponding to a CE value of $\approx 99.9\%$. On the other hand, highly functionalized CCMs suffer from poor cycling stability because the carbon surface degrades with cycling.^[19,20] Although the deterioration of the cycle life can be retarded using more ordered graphitic materials, their enhanced crystallinity has other disadvantages, such as reduced number of active sites and poor wettability for the electrolyte.^[19] In addition, a decrease in the number of lithiophilic/sodiophilic sites can lead to unexpected cycling off and large deviation of the CE values. A new template material with stronger but more numerous catalytic sites is required to achieve a better anode-free SMB with high electrochemical performance.

In this study, a silver nanofiber@nitrogen-rich carbon thin layer core-shell material (SNF@NCL) was prepared for use in anode-free SMBs using a simple polyol method, which was followed by low-temperature heating. The SNF@NCL with a high aspect ratio of >1500 (diameter: ≈ 55 nm, length: >100 μm) was deposited as a thin nanoweb structure on an Al current collector. The macroporous nanoweb (MP-NWB) composed of SNF@NCL had a high electroconductivity of >80 S cm^{-1} as well as a large number of sodiophilic sites, showing exceptionally high electrochemical performance for reversible sodium metal storage. In particular, significantly long and stable cycling behavior was sustained for 1600 cycles. Moreover, in a revived cycling test, this enhanced cycling performance was maintained

for additional 1500 cycles with mean CEs of $>99.9\%$. These results show that anode-less SMBs with nanohybrid templates can be practical in the near future.

2. Results and Discussion

The morphologies of SNF@NCLs were confirmed by field emission scanning electron microscopy (FE-SEM), as shown in **Figure 1a** and **Figure S1** (Supporting Information). The SNF@NCLs had uniform diameters of ≈ 55 nm and lengths of more than ≈ 100 μm (aspect ratio >1500), and their stacking led to a 3D macroporous nanoweb structure. In addition, the cross-sectional SEM image for the fractured surface of MP-NWBs revealed a thickness of ≈ 5 μm (**Figure S2**, Supporting Information). High-resolution transmission electron microscopy (HR-TEM) revealed the presence of a few-nanometer-sized coating layer on the surface of the SNFs (**Figure 1b**). The thin layer was amorphous and highly defective, whereas the inside of the coating layer was a well-ordered crystal structure (**Figure 1b**). The selective area diffraction pattern indicated that the crystalline core is a well-ordered silver metal (inset of **Figure 1b**). X-ray diffraction (XRD) supports the high crystallinity of SNFs (**Figure 1c**), where a sharp silver (111) peak as well as other silver (200), (220), (311), and (222) peaks were confirmed at 38.1° , 44.8° , 64.8° , 77.3° , and

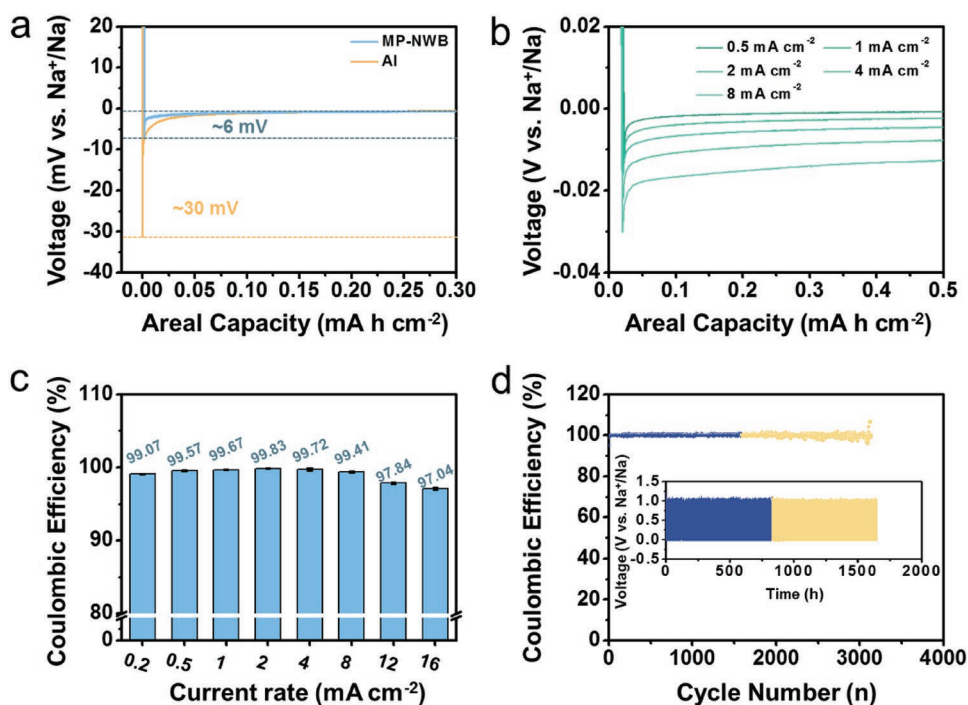


Figure 2. Electrochemical performance of MP-NWB-based sodium metal anode with a cut-off capacity of 0.5 mA h cm^{-2} . a) Galvanostatic discharge profile of MP-NWB- and Al-based metal anodes at a current rate of $50 \mu\text{A cm}^{-2}$, b) rate performance data characterized at a current range from 0.5 to 8 mA cm^{-2} , c) average CE values and standard deviation at different current rates, and d) cycling performances over ≈ 1600 cycles and followed by 1500 cycles and inset of time versus voltage profiles for cycling.

$81.7^\circ 2\theta$, respectively. The chemical composition of the amorphous layers and SNFs was characterized by X-ray photoelectron spectroscopy (XPS) (Figure 1d–f). As shown in the C 1s spectrum, sp^2 C=C bonding at 284.4 eV and sp^3 C–C bonding at 284.8 eV were observed in the amorphous layer, and a large amount of C–N functional groups were also noted at 286.3 eV (Figure 1d).^[35] In the case of nitrogen groups, the main bonding peak was found at 396.7 eV in the N 1s spectrum, indicating a pyridinic structure (N-6) (Figure 1e).^[36] These results suggest that the surface coating layer is composed of conjugated polyhexagonal carbon materials. In addition, the Ag 3d spectrum exhibited a doublet of $Ag3d_{5/2}$ and $Ag3d_{3/2}$ at 368.1 and 374.1 eV , respectively, corresponding to the Ag^0 structure (Figure 1f). The contents of nitrogen and silver were calculated to be C/N and C/Ag ratio of 5.3 and 2.2 , respectively. These results also suggest that the carbon layer is so thin that a large number of core atoms can be detected. Numerous nitrogen dopants were observed on the edge site of the polyhexagonal carbon structure. Nitrogen functional groups are the active sites for sodium ion chemisorption, which can act as a sodiophilic moiety, leading to catalytic effects for sodium metal deposition/dissolution process. In addition, high aspect ratio of SNF networks can deliver electrons quite rapidly, of which electrical conductivity characterized by a four-probe method corresponds to a high electrical conductivity of $\approx 80 \text{ S cm}^{-1}$. Therefore, MP-NWBs can be an ideal catalytic nanotemplate for reversible sodium metal storage cycles because the sodiophilic shell can collect sodium ions and the strong and conducting metal core can not only endure repetitive metal deposition/dissolution cycling, but also transfer electrons rapidly.

Galvanostatic sodium metal deposition/dissolution tests were conducted in a diglyme-based electrolyte containing 1 M NaPF_6 with a cut-off capacity of 0.5 mA h cm^{-2} . As shown in Figure 2a, the first discharge profile of the MP-NWBs at a current rate of $50 \mu\text{A cm}^{-2}$ revealed a voltage overshoot (VO), which is observed typically when metal deposition occurs due to the nucleation energy barrier. The VO of MP-NWBs was $\approx 6 \text{ mV}$, which was one-fifth that ($\approx 30 \text{ mV}$) of bare Al foil (Figure 2a). The highly reduced VO of MP-NWBs demonstrated the catalytic effects of MP-NWBs. With increasing current rate, the VO values increased gradually from ≈ 6 to $\approx 15 \text{ mV}$, which are still much smaller than those of other reported catalytic materials (Figure 2b).^[19,20,32–34] These results highlight the superior kinetic performance of MP-NWBs. The high electrical conductivity of MP-NWBs and large number of catalytic sites could lead to the high rate capabilities by the areal current rate of 8 mA cm^{-2} . One noteworthy result was the significantly high CE values over a wide range of current rates (Figure 2c). At 0.2 mA cm^{-2} , average CEs of $\approx 99.07\%$, corresponding to an areal capacity of $495.35 \text{ mA h cm}^{-2}$, were achieved. The average CEs increased gradually to $\approx 99.83\%$ ($499.15 \text{ mA h cm}^{-2}$) by 2 mA cm^{-2} , and $> 99\%$ was maintained by a high areal current rate of 8 mA cm^{-2} . Basically, when a low current density was applied to galvanostatic metal deposition/stripping cycling, the CE values decreased significantly because the reduced kinetic barriers for a side reaction accelerate the formation of several byproducts. In particular, nanostructured carbon-based catalytic templates experience considerably more severe deterioration of the CE values because of their high specific surface area. In addition, the excessively high current densities

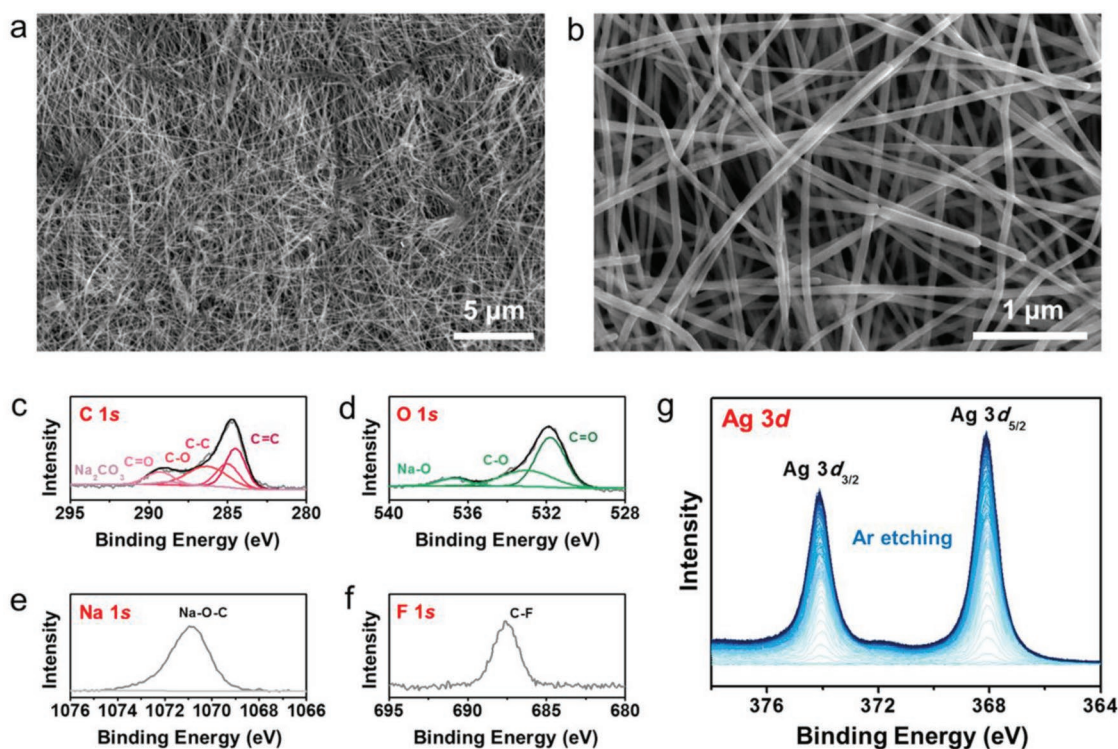


Figure 3. Ex situ characterization data of MP-NWBs-based sodium metal anode after 500 cycles. a,b) FE-SEM images at different magnifications, XPS c) C 1s, d) O 1s, e) Na 1s, and f) F 1s spectra, and g) XPS depth profiles of Ag 3d spectra characterized with Ar etching.

cause diffusion-controlled metal deposition accompanying dendrite-like structures.^[20] As a result, despite the use of catalytic template materials, film-like metal growth governed by a kinetic-controlled mechanism is allowed in a limited current density range. To expand the feasible current ranges, it is very important to mitigate the continuous degradation of both the electrolyte and electrode materials as well as improve the kinetic performance. The core material (SNF) in MP-NWBs has a highly rigid physicochemical property, which could undergo neither volume changes nor corrosion during repetitive cycling. In addition, their network structures can deliver electrons to every hole and corner quite rapidly.

The solidity of SNF and its network structure were confirmed by ex situ SEM characterization after 500 cycles (Figure 3a–c). As shown in the ex situ SEM images, the original macroporous web structures were well-maintained (Figure 3a), but the mean fiber diameter of ≈ 55 nm had increased slightly to ≈ 80 nm after long-term cycling (Figure 3b). Note that there are few byproducts after 500 repetitive cycles, which is in contrast to the ex situ SEM images of the bare Al electrode without MP-NWBs, as shown in the ex situ SEM image (Figure S3, Supporting Information). The increased diameter on MP-NWBs could be due mainly to the formation of solid electrolyte interface (SEI) layers and the small quantity of inactive byproducts. An ex situ XPS test was conducted to characterize the surface properties of SNF@NCLs further after the cycling test (Figure 3c–f). In the ex situ C 1s spectrum, new C–O, C=O, and Na_2CO_3 bonds were confirmed at 286.3, 288.5, and 289.3 eV, respectively (Figure 3c). The ex situ O 1s spectrum coincided with the result in C 1s, where C=O and C–O bonds

were observed at 531.8 and 533.1 eV, respectively (Figure 3d). In addition, Na–O–C and C–F bonding were detected in the Na 1s and F 1s spectra, respectively (Figure 3e,f). These ex situ results confirmed that the carbon shell plays a key role in forming a SEI layer and mitigating the formation of byproducts. In contrast, the core SNF was well-maintained in the repetitive discharge/charge loops, which was confirmed in ex situ XPS depth profiles with Ar etching (Figure 3g). The intensity of the doublet of $\text{Ag}3d_{5/2}$ and $\text{Ag}3d_{3/2}$ at 368.1 and 374.1 eV, respectively, increased significantly with increasing etching depth, and the doublet peak was not changed, indicating the rigidity of SNFs. As a result, when the MP-NWBs were used as a catalytic template, high average CE values of $>99\%$ were achieved over a wide range of currents from 0.2 to 8 mA cm^{-2} . In addition, MP-NWBs worked for a very long time with stable CEs $>99.9\%$ during repetitive cycling for more than ≈ 1600 cycles (Figure 2d), and the cycle life stopped suddenly without symptoms despite the similar galvanostatic sodium metal plating/stripping curves at the initial and 1600th cycles (Figure S4, Supporting Information). To understand the origin of the unexpected end of the cycle life, the MP-NWBs recovered from the tested cells after ≈ 1600 cycles were reassembled with a new sodium metal counter/reference electrode and the same electrolyte. Interestingly, the reassembled cell worked for an additional ≈ 1500 cycles, and the average CE values were similar to those of the previous test (Figure 2d). This result highlights the importance of catalytic electrode materials for reversible sodium metal storage. In a previous study, a carbonaceous thin film, which has a large number of oxygen and nitrogen functional groups, was coated on Cu foil and used

as a catalytic seed layer to assist homogeneous metal plating/dissolution cycling.^[37] The thin film reduced the voltage overshoot and overpotential by ≈ 10 mV, which was lower than those reported for nitrogen and sulfur codoped carbon nanotube paper^[38] and carbon black film coated on Al foil^[34] (≈ 9 mV and ≈ 12 mV, respectively), leading to the highest CEs of $> 99.9\%$ in the reported results.^[16–20,32,34,37,38] On the other hand, the amorphous carbon-based thin film degraded gradually after repetitive metal plating/dissolution cycling for more than 300 cycles, indicating that more rigid carbon materials are required to achieve more stable cycling performance. In contrast, a more ordered carbon-based film coated on Al foil and graphitic carbon nanotemplates could endure more than 1000 cycles with relatively low CEs of $\approx 99.8\%$.^[19,34] These results suggest that a more rigid electrode material with a larger number of catalytic sites is required to achieve both higher CEs and longer cycling stabilities. The SNF@NCLs can not only provide multitudinous catalytic sites for sodium metal nucleation, but also endure significantly long-term cycling by the effects of catalytic shell and rigid core. Therefore, the MP-NWBs composed of SNF@NCLs could show the exceptionally long-term cycling performance for more than 3000 cycles with a high CE of $\approx 99.9\%$. In addition, the stable cycling performances was maintained at higher cut-off areal capacities of 2.0 and 4.0 mA h cm⁻² (Figure S5, Supporting Information).

To confirm the catalytic effects of the NCL on the electrochemical performance of SNF@NCLs, a nitrogen-rich hollow carbon material, a few nanometers in thickness, was prepared from polyvinylpyrrolidone (PVP) and silica using a previously reported method (Figure S6a, Supporting Information).^[39] The VO value of the nitrogen-rich carbon coated on Al foil was ≈ 7 mV, which was similar to that observed for SNF@NCLs (Figure S6c, Supporting Information). In the galvanostatic sodium metal deposition/stripping cycling tests, stable cycles were achieved for up to 150 cycles (Figure S6d, Supporting Information). On the other hand, after 150 cycles, the CE values fluctuated and cycling was suddenly dead (Figure S6d, Supporting Information). The abrupt interruption of the cycling behaviors could be induced by the degradation of the carbon materials with repetitive cycling. For comparison, SNFs without the NCLs were prepared and their electrochemical performance was also tested under the same conditions (Figure S6b–d, Supporting Information). In the initial sodium metal plating process, despite their high surface area similar to that of SNF@NCLs, the carbon-free SNFs showed a significantly high VO value of ≈ 18 mV. In addition, the carbon layer-free SNFs showed unstable cycling behaviors with poor CEs (Figure S6d, Supporting Information). These results support the indispensability of both the SNF and NCL for achieving high electrochemical performance. Moreover, the thickness of NCLs was controlled by introducing a summative PVP coating layer during the heating process, where the effects of the coating thickness on the electrochemical performance were investigated (Figure S7, Supporting Information). Despite the change in the thickness of the NCLs, stable cycling performance similar to the original one were well-maintained for more than 300 cycles, suggesting that the thickness of the carbon layer has an insignificant effect (Figure S7, Supporting Information).

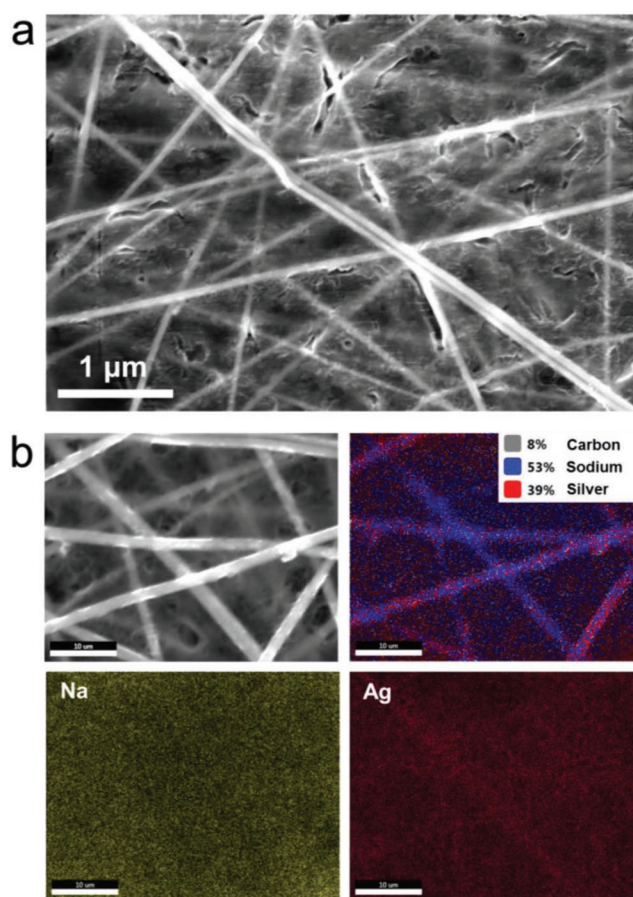


Figure 4. Ex situ a) FE-SEM image and b) EDS mapping data of MP-NWBs-based sodium metal anode after sodium metal deposition by an areal capacity of 0.5 mA h cm⁻².

Dendritic metal-free sodium metal deposition behavior on MP-NWBs was characterized further by ex situ SEM and energy dispersive spectroscopy (EDS) (Figure 4). After sodium metal deposition by an areal capacity of 0.5 mA h cm⁻², a metal-filled network structure of SNF@NCLs was observed (Figure 4a). Although the deposited metal had been damaged by the strong energy of the electron beam, a dendrite-free morphology was confirmed in the SEM image (Figure 4a). EDS mapping data also show that sodium metal had been introduced homogeneously in the overall area of the SNF@NCL networks (Figure 4b). The dendrite-free metal plating/stripping cycles could lead to stable cycling performance with exceptionally high CEs. The ascendancy of MP-NWBs on the sodium metal deposition/extraction cycles are described schematically in Figure S8 (Supporting Information).

To demonstrate the practicability of anode-free sodium metal batteries (AF-SMBs) based on MP-NWBs, a high-performance active material, Na_{1.5}VPO_{4.8}F_{0.7}, was used as cathode for the full cells.^[40] The respective MP-NWB and Na_{1.5}VPO_{4.8}F_{0.7} were precycled for 10 cycles, and full cells were then assembled using the precycled MP-NWB to a Na_{1.5}VPO_{4.8}F_{0.7} mass ratio of 15%. The Na_{1.5}VPO_{4.8}F_{0.7} cathode delivered a reversible capacity of ≈ 108 mA h g_{cathode}⁻¹ at a voltage of 3.84 V using the excessive sodium metal counter/reference electrode (Figure 5a).

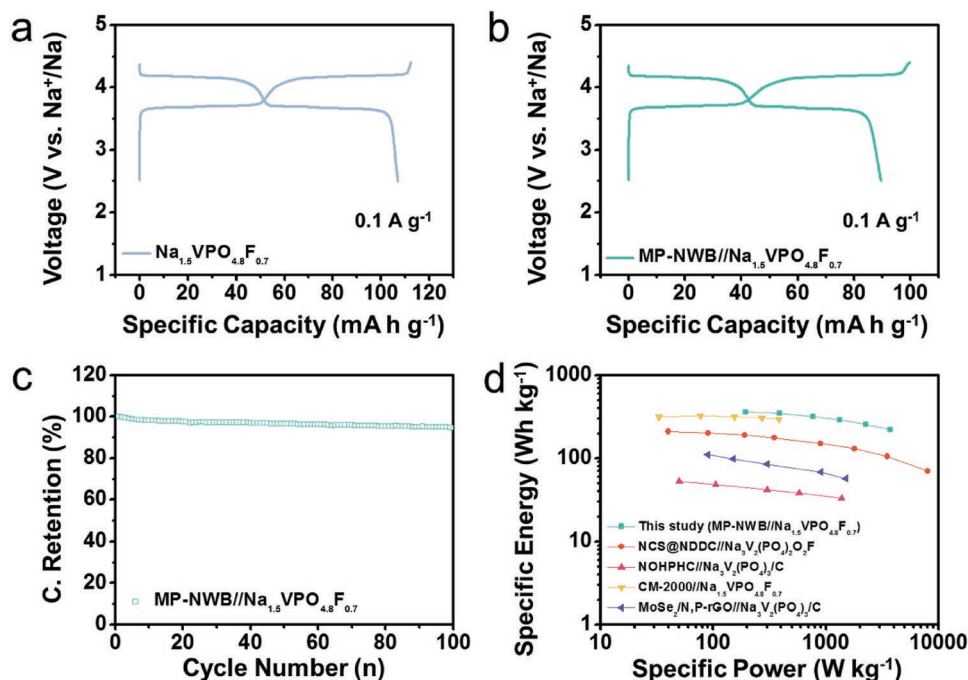


Figure 5. Electrochemical performance of AF-SMBs based on MP-NWBs over a voltage window of 2.5–4.4 V assembled after precycling of both the anode and cathode. Galvanostatic charge/discharge profiles of a) $\text{Na}_{1.5}\text{VPO}_{4.8}\text{F}_{0.7}$ cathode in a half-cell configuration with an excessive sodium metal reference/counter electrode and b) AF-SMBs in a full cell configuration with a MP-NWB template. c) Cycling behaviors of AF-SMBs over 100 cycles and d) Ragone plots of several energy storage devices including AF-SMBs.

Although the specific capacity was a little reduced due to the increase in the calculated electrode weight (both anode and cathode), a similar profile was observed in the NP-NWB// $\text{Na}_{1.5}\text{VPO}_{4.8}\text{F}_{0.7}$ cells (Figure 5b), which can be possible by precycling. Because the initial irreversible capacities were removed effectively during the initial precycling step, a similar profile to the intrinsic sodium ion storage capacity of the cathode was achieved. Figure S9 (Supporting Information) shows the poor charge/discharge properties of the NP-NWB// $\text{Na}_{1.5}\text{VPO}_{4.8}\text{F}_{0.7}$ cell tested without pre-cycling. In the cycling test of NP-NWB// $\text{Na}_{1.5}\text{VPO}_{4.8}\text{F}_{0.7}$ cells, the limited sodium ions can be stored reversibly for 100 cycles (Figure 5c). Approximately 95% of the initial capacity had been retained after 100 cycles, exhibiting the high CEs of the NP-NWB// $\text{Na}_{1.5}\text{VPO}_{4.8}\text{F}_{0.7}$ cells. The cycling performance of NP-NWB// $\text{Na}_{1.5}\text{VPO}_{4.8}\text{F}_{0.7}$ cells surpassed that of the previously reported results, such as carbon/Al//pyrite and MC-CNT-2400// $\text{Na}_{1.5}\text{VPO}_{4.8}\text{F}_{0.7}$.^[19,34] The carbon/Al//pyrite showed a capacity retention of $\approx 85\%$ after 40 cycles,^[34] and MC-CNT-2400// $\text{Na}_{1.5}\text{VPO}_{4.8}\text{F}_{0.7}$ maintained $\approx 90\%$ of the initial capacity after 25 cycles.^[19] Moreover, the energy and power performance of the anode-free full cells were superior to those of other full cells (Figure 5d).^[41–44] A high specific energy of $\approx 380 \text{ Wh kg}_{\text{electrode}}^{-1}$ at $\approx 190 \text{ W kg}_{\text{electrode}}^{-1}$ as well as a high specific power of $\approx 3700 \text{ W kg}_{\text{electrode}}^{-1}$ at $\approx 220 \text{ Wh kg}_{\text{electrode}}^{-1}$ were demonstrated.

3. Conclusion

In summary, a SNF@NCL was prepared from a simple polyol method followed by low-temperature heating, and deposited on

an Al current collector as a thin nanoweb structure. The NCL shell had a thickness in the few-nanometer-scale, an amorphous carbon structure and a large number of nitrogen functional groups (C/N ratio of 5.3), whereas the bulk SNF core had a highly ordered crystal structure and a high aspect ratio of >1500 . The MP-NWBs exhibited a high electrical conductivity of $\approx 80 \text{ S cm}^{-1}$. When the MP-NWBs were used as a catalytic template for sodium metal storage, the VO for sodium metal nucleation was reduced significantly to $\approx 6 \text{ mV}$, and a practicable operating current range was expanded to between 0.2 and 8.0 mA cm^{-2} . In addition, high average CEs of $\approx 99\%$ were achieved in the expanded current ranges. Moreover, MP-NWBs showed remarkably stable and long cycling performance with CEs of $>99.9\%$ during ≈ 1600 cycles and an additional ≈ 1500 cycles. In a full cell test with a polyanion cathode material, the MP-NWBs-based full cells possessed a high specific energy of $\approx 380 \text{ Wh kg}_{\text{electrode}}^{-1}$ at $\approx 190 \text{ W kg}_{\text{electrode}}^{-1}$ and a high specific power of $\approx 3700 \text{ W kg}_{\text{electrode}}^{-1}$ at $\approx 220 \text{ Wh kg}_{\text{electrode}}^{-1}$. Furthermore, the AF-SMBs based on SNF@NCL proved their feasibility over 100 cycles, showing $\approx 95\%$ retention of the initial capacity.

4. Experimental Section

Preparation of SNF@NCL and MP-NWBs: The high aspect ratio SNF@NCLs were prepared according to the methodology reported elsewhere based on successive multistep growth using repetitive AgNO_3 reduction in an ethylene glycol (EG) solution with PVP.^[45] PVP is a precursor of the polyhexagonal carbon layer, which was injected in the respective steps for metal growth. In the procedure, the fabricated SNFs were heated in EG media with PVP in a closed chamber at

≈180 °C, where a few-nanometer scale NCLs were introduced to the SNFs by the thermal decomposition of PVP without a further step. To prepare the SNF@NCL nanohybrid template, the as-prepared SNF@NCL dispersion in ethylene glycol was vacuum-filtered on a porous alumina membrane filter (47 mm diameter, 0.2 μm pore size; Whatman). After drying in a vacuum chamber at 30 °C for 12 h, the SNF@NCL nanohybrid template on the alumina filter was pressed on Al foil. The resulting MP-NWBs (nanohybrid template) were stored in a vacuum chamber at 30 °C.

Characterization and Electrochemical characterization methods were included in the Supporting Information.

Supporting Information

Supporting Information is available from the Wiley Online Library or from the author.

Acknowledgements

This research was supported by the Basic Science Research Program through the National Research Foundation of Korea (NRF) funded by the Ministry of Education (Nos. 2017R1C1B1004167 and 2018R1A4A1025169).

Conflict of Interest

The authors declare no conflict of interest.

Keywords

anode-free, core-shell, metal batteries, nanohybrid, nitrogen-doped carbon

Received: March 11, 2019

Revised: July 4, 2019

Published online: July 18, 2019

- [1] P. Nejat, F. Jomehzadeh, M. M. Taheri, M. Gohari, M. Z. A. Majid, *Renewable Sustainable Energy Rev.* **2015**, *43*, 843.
- [2] M. Bhattacharya, S. R. Paramati, I. Ozturk, S. Bhattacharya, *Appl. Energy* **2016**, *162*, 733.
- [3] S. Chu, Y. Cui, N. Liu, *Nat. Mater.* **2017**, *16*, 16.
- [4] O. Ellabban, H. Abu-Rub, F. Blaabjerg, *Renewable Sustainable Energy Rev.* **2014**, *39*, 748.
- [5] D. Larcher, J.-M. Tarascon, *Nat. Chem.* **2015**, *7*, 19.
- [6] A. Kwade, W. Haselrieder, R. Leithoff, A. Modlinger, F. Dietrich, K. Droeder, *Nat. Energy* **2018**, *3*, 290.
- [7] J. K. Stolaroff, C. Samaras, E. R. O'Neill, A. Lubers, A. S. Mitchell, D. Ceperley, *Nat. Commun.* **2018**, *9*, 409.
- [8] G. Zheng, S. W. Lee, Z. Liang, H.-W. Lee, K. Yan, H. Yao, H. Wang, W. Li, S. Chu, Y. Cui, *Nat. Nanotechnol.* **2014**, *9*, 618.
- [9] A. C. Kozen, C.-F. Lin, A. J. Pearse, M. A. Schroeder, X. Han, L. Hu, S.-B. Lee, G. W. Rubloff, M. Noked, *ACS Nano* **2015**, *9*, 5884.
- [10] N.-W. Li, Y.-X. Yin, C.-P. Yang, Y.-G. Guo, *Adv. Mater.* **2016**, *28*, 1853.
- [11] G. Zheng, C. Wang, A. Pei, J. Lopez, F. Shi, Z. Chen, A. D. Sendek, H.-W. Lee, Z. Lu, H. Schneider, M. M. Safont-Sempere, S. Chu, Z. Bao, Y. Cui, *ACS Energy Lett.* **2016**, *1*, 1247.
- [12] H.-R. Yao, P.-F. Wang, Y. Gong, J. Zhang, X. Yu, L. Gu, C. Ouyang, Y.-X. Yin, E. Hu, X.-Q. Yang, E. Stavitski, Y.-G. Guo, L.-J. Wan, *J. Am. Chem. Soc.* **2017**, *139*, 8440.
- [13] C. Wang, L. Wang, F. Li, F. Cheng, J. Chen, *Adv. Mater.* **2017**, *29*, 1702212.
- [14] G. Yoon, H. Kim, I. Park, K. Kang, *Adv. Energy Mater.* **2017**, *7*, 1601519.
- [15] Y. S. Yun, K.-Y. Park, B. Lee, S. Y. Cho, Y.-U. Park, S. J. Hong, B. H. Kim, H. Gwon, H. Kim, S. Lee, Y. W. Park, H.-J. Jin, K. Kang, *Adv. Mater.* **2015**, *27*, 6914.
- [16] W. Luo, C.-F. Lin, O. Zhao, M. Noked, Y. Zhang, G. W. Rubloff, L. Hu, *Adv. Energy Mater.* **2017**, *7*, 1601526.
- [17] Y.-J. Kim, H. Lee, H. Noh, J. Lee, S. Kim, M.-H. Ryou, Y. M. Lee, H.-T. Kim, *ACS Appl. Mater. Interfaces* **2017**, *9*, 6000.
- [18] Y. Zhao, L. V. Goncharova, A. Lushington, Q. Sun, H. Yadegari, B. Wang, W. Xiao, R. Li, X. Sun, *Adv. Mater.* **2017**, *29*, 1606663.
- [19] H. J. Yoon, N. R. Kim, H.-J. Jin, Y. S. Yun, *Adv. Energy Mater.* **2018**, *8*, 1701261.
- [20] H. J. Yoon, S. K. Hong, M. E. Lee, J. Hwang, H.-J. Jin, Y. S. Yun, *ACS Appl. Energy Mater.* **2018**, *1*, 1846.
- [21] M. Wang, C. Jiang, S. Zhang, X. Song, Y. Tang, H.-M. Cheng, *Nat. Chem.* **2018**, *10*, 667.
- [22] I. A. Rodríguez-Pérez, Y. Yuan, C. Bommier, X. Wang, L. Ma, D. P. Leonard, M. M. Lerner, R. G. Carter, T. Wu, P. A. Greaney, J. Lu, X. Ji, *J. Am. Chem. Soc.* **2017**, *139*, 13031.
- [23] D.-Y. Wang, C.-Y. Wei, M.-C. Lin, C.-J. Pan, H.-L. Chou, H.-A. Chen, M. Gong, Y. Wu, C. Yuan, M. Angell, Y.-J. Hsieh, Y.-H. Chen, C.-Y. Wen, C.-W. Chen, B.-J. Hwang, C.-C. Chen, H. Dai, *Nat. Commun.* **2017**, *8*, 14283.
- [24] H.-D. Lim, B. Lee, Y. Zheng, J. Hong, J. Kim, H. Gwon, Y. Ko, M. Lee, K. Cho, K. Kang, *Nat. Energy* **2016**, *1*, 16066.
- [25] Y. Bae, Y. S. Yun, H.-D. Lim, H. Lee, Y.-J. Kim, J. Kim, H. Park, Y. Ko, S. Lee, H. J. Kwon, H. Kim, H.-T. Kim, D. Im, K. Kang, *Chem. Mater.* **2016**, *28*, 8160.
- [26] L. Lutz, D. A. D. Corte, Y. Chen, D. Batuk, L. R. Johnson, A. Abakumov, L. Yate, E. Azaceta, P. G. Bruce, J.-M. Tacascon, A. Grimaud, *Adv. Energy Mater.* **2018**, *8*, 1701581.
- [27] N. Xiao, X. Ren, W. D. McCulloch, G. Gourdin, Y. Wu, *Acc. Chem. Res.* **2018**, *51*, 2335.
- [28] J.-S. Lee, G. Nam, J. Sun, S. Higashi, H.-W. Lee, S. Lee, W. Chen, Y. Cui, J. Cho, *Adv. Energy Mater.* **2016**, *6*, 1601052.
- [29] X. Wei, W. Xu, J. Hwang, L. Zhang, E. Walter, C. Lawrence, M. Vijayakumar, W. A. Henderson, T. Liu, L. Cosimbescu, B. Li, V. Sprenkle, W. Wang, *Angew. Chem., Int. Ed.* **2015**, *54*, 8684.
- [30] N. Yabuuchi, K. Kubota, M. Dahbi, S. Komaba, *Chem. Rev.* **2014**, *114*, 11636.
- [31] R. Miao, J. Yang, Z. Xu, J. Wang, Y. Nuli, L. Sun, *Sci. Rep.* **2016**, *6*, 21771.
- [32] Z. W. Seh, J. Sun, Y. Sun, Y. Cui, *ACS Cent. Sci.* **2015**, *1*, 449.
- [33] R. Zhang, X.-R. Chen, X. Chen, X.-B. Cheng, X.-Q. Zhang, C. Yan, Q. Zhang, *Angew. Chem., Int. Ed.* **2017**, *56*, 7764.
- [34] A. P. Cohn, N. Muralidharan, R. Carter, K. Share, C. L. Pint, *Nano Lett.* **2017**, *17*, 1296.
- [35] J. H. Choe, J. Jeon, M. E. Lee, J. J. Wie, H.-J. Jin, Y. S. Yun, *Nanoscale* **2018**, *10*, 2025.
- [36] S. Y. Cho, Y. S. Yun, S. Lee, D. Jang, K.-Y. Park, J. K. Kim, B. H. Kim, K. Kang, D. L. Kaplan, H.-J. Jin, *Nat. Commun.* **2015**, *6*, 7145.
- [37] M. E. Lee, H. W. Kwak, J. H. Kwak, H.-J. Jin, Y. S. Yun, *ACS Appl. Mater. Interfaces* **2019**, *11*, 12401.
- [38] B. Sun, P. Li, J. Zhang, D. Wang, P. Munroe, C. Wang, P. H. L. Notten, G. Wang, *Adv. Mater.* **2018**, *30*, 1801334.
- [39] Y. S. Yun, S. Y. Cho, H. Kim, H.-J. Jin, K. Kang, *ChemElectroChem* **2015**, *2*, 359.

- [40] Y. U. Park, D.-H. Seo, H.-S. Kwon, B. Kim, J. Kim, H. Kim, I. Kim, H.-I. Yoo, K. Kang, *J. Am. Chem. Soc.* **2013**, *135*, 13870.
- [41] P. Lee, J. Lee, H. Lee, J. Yeo, S. Hong, K. H. Nam, D. Lee, S. S. Lee, S. H. Ko, *Adv. Mater.* **2012**, *24*, 3326.
- [42] B.-H. Hou, Y.-Y. Wang, D.-S. Liu, Z.-Y. Gu, X. Feng, H. Fan, T. Zhang, C. Lu, X.-L. Wu, *Adv. Funct. Mater.* **2018**, *28*, 1805444.
- [43] M. Huang, B. Xi, Z. Feng, J. Liu, J. Feng, Y. Qian, S. Xiong, *J. Mater. Chem. A* **2018**, *6*, 16465.
- [44] J. Choi, M. E. Lee, S. Lee, H.-J. Jin, Y. S. Yun, *ACS Appl. Energy Mater.* **2019**, *2*, 1185.
- [45] F. Niu, J. Yang, N. Wang, D. Zhang, W. Fan, J. Yang, Y. Qian, *Adv. Funct. Mater.* **2017**, *27*, 1700522.